ELSEVIER

Journal of South American Earth Sciences 25 (2008) 298–312

Journal of
South American
Earth Sciences

www.elsevier.com/locate/jsames

Sr–Nd isotopic evidence for crustal contamination in the Niquelândia complex, Goiás, Central Brazil

Giorgio Rivalenti [a,*], Ciro T. Correia [b], Vicente A.V. Girardi [b], Maurizio Mazzucchelli [a], Colombo C.G. Tassinari [b], Gustavo W. Bertotto [c]

[a] *Dipartimento di Scienze della Terra, Università di Modena e Reggio Emilia, P.le S. Eufemia 19, 41100 Modena, Italy*
[b] *Instituto de Geociências, Universidade de São Paulo, Rua do Lago 563, Cidade Universitaria 05508-900, São Paulo, Brazil*
[c] *Conicet And Facultad De Ciencias Exactas Y Naturales, Universidad Nacional De La Pampa, Uruguay 151, 6300 Santa Rosa, La Pampa, Argentina*

Received 5 April 2007; accepted 31 August 2007

Abstract

The Niquelândia complex is a Neoproterozoic mafic-ultramafic intrusion resulting from fractional crystallization of primary picritic basalt intrusions. It consists of two layered sequences: a lower and larger one (LS), where four stratigraphic units exhibit an upward decrease of ultramafic layers and increase of gabbroic layers; an upper, smaller sequence (US), separated from LS by a high-temperature shear zone and consisting of two stratigraphic units (gabbros + anorthosites and amphibolites). Nd and Sr isotopic analyses and rare earth element (REE) profiles provide evidence that the complex suffered important crustal contamination. The LS isotopic array trends from a DM region with positive εNd and moderately positive εSr towards a field occupied by crustal xenoliths, especially abundant in the upper LS (negative εNd and large, positive εSr). Each LS stratigraphic unit is distinct from the next underlying unit, showing lower εNd and higher εSr, suggesting inputs of fresh magma and mixing with the contaminated, residual magma. The US is characterised by a relatively high variation of εNd and constant εSr. REE patterns vary within each unit from LREE depleted to LREE enriched in the samples having lower εNd and higher εSr. The contamination process has been modelled by using the EC-AFC algorithms from [Spera, F.J., Bohrson, W.A., 2001. Energy-constrained open-system magmatic processes I: general model and energy-constrained assimilation and fractional crystallization (EC-AFC) formulation. J. Petrology 42, 999–1018]. The differences between the LS and US isotopic arrays are consistent with contamination by the same crustal component, provided that its melting degree was higher in LS than in US. The different degrees of anatexis are explained by the heat budget released from the magma, higher in LS (because of its larger mass) than in US. Comparison of the correlations between isotopes and incompatible trace element ratios of the models and of the gabbros shows some differences, which are demonstrably related with the variable amount of cumulus phases and trapped melt in the gabbros.

Keywords: Niquelândia; Layered complex; EC-AFC; Crustal contamination

1. Introduction

Crustal contamination is an important process in most layered intrusions (e.g., Ivrea-Verbano, Voshage et al., 1990; Sinigoi et al., 1991; Bushweld, Eales and Cawthorn, 1996; Lee, 1996; Great dyke, Lee, 1996; Skaergaard, McBirney, 1996; various complexes in Norway, Wilson et al., 1996; Wilson and Sorensen, 1996; Nielsen et al., 1996; Rum, Emeleus et al., 1996; Stillwater, Mc Callum, 1996). This is the logical consequence of the heating, up to anatexis, of the wall rocks induced by the crystallization of a large magma mass. As reviewed by Lee (1996), crustal contamination may exert an important control also on the type and localization of economic mineral deposits (e.g. Buchanan and Rouse, 1984).

With its approximately 1100 km^2, Niquelândia is one of the largest layered massifs in South America and the major

* Corresponding author. Tel.: +39 59 205 5813; fax: +39 59 205 5887.
E-mail address: riva@unimore.it (G. Rivalenti).

0895-9811/$ - see front matter © 2007 Elsevier Ltd. All rights reserved.
doi:10.1016/j.jsames.2007.08.007

source for economic Ni deposits. Such a large igneous intrusion must have induced important heating of the country crustal rocks, with a high probability to become thereafter contaminated. While several studies have dealt with its stratigraphy, petrology and isotope geochemistry and age of emplacement, there is no systematic study, except our previous report (Girardi et al., 2006a), aimed to constrain the contamination process. Crustal contamination, however, has been qualitatively recognised in a portion of the Niquelândia complex containing abundant crustal xenoliths (Ferreira Filho et al., 1998; Pimentel et al., 2004, 2006). In this study we provide Sr and Nd isotopic evidence that crustal contamination occurred all through the complex by variable mechanisms and variable geochemical results, dominantly depending on melt volume, related heat budget and induced anatexis degree. A direct consequence of crustal contamination is that it provides an easy explanation for the frustrating attempts and contrasting results in inferring an emplacement age of the Niquelândia complex from the Sr and Nd isotope systematics.

2. Geological setting, stratigraphy, petrography and age

The Niquelândia layered intrusion, together with the Cana Brava and Barro Alto complexes, form a 350 km long, NNE–SSW elongated belt in Central Goias, Brazil, between the São Francisco and Amazonian Cratons. These mafic-ultramafic stratiform complexes are part of the Goiás Massif, a complex geotectonic unit constituted mainly by Archean and Proterozoic rocks, belonging to the Tocantins Province (Pimentel et al., 2004).

According to Rivalenti et al. (1982) and Girardi et al. (1986), the Niquelândia complex consists of a lower (LS) and an upper (US) layered sequence separated by a high temperature shear zone which contains abundant crustal xenoliths and lenses (Fig. 1). US is in igneous contact with the volcano-sedimentary Proterozoic Indaianópolis sequence (Nascimento et al., 1981; Brod and Jost, 1991) and LS is in tectonic contact with the terrains of the Paleoproterozoic basement.

LS consist of four stratigraphic units, from bottom (at the East) upwards, BGZ (gabbronorite, pyroxenite, peridotite), BPZ (peridotite and minor pyroxenite), LUZ (peridotite, pyroxenite and minor gabbronorite) and LGZ (dominant gabbronorites and minor pyroxenite). The gabbro norites at the top of LGZ contain biotite, hornblende, apatite and zircon and are enriched in incompatible elements and LREE. This region was designated as "hydrous zone" by Girardi et al. (1986). Detailed mapping of this zone revealed the abundant presence of country-rocks xenoliths from the volcano-sedimentary Indaianópolis sequence (Girardi et al., 2006a).

US consists of two stratigraphic units, from bottom upward UGAZ (gabbro and anorthosite) and UA (amphibolites), which constitute the roof at the West.

Rivalenti et al. (1982) inferred that the crystallization sequence was olivine (ol), spinel (sp), orthopyroxene (opx), clinopyroxene (cpx), plagioclase (pl) in BGZ, sp-ol-opx in BPZ, ol-cpx-opx-pl in LUZ, and cpx-pl-opx in LGZ, whereas it was ol-cpx-pl in UGAZ and amphibole (amph) $\pm$ cpx $-$ pl in UA, approaching the equilibrium crystallization of a hydrous melt residue.

Rivalenti et al. (1982) and Girardi et al. (1986) concluded that the different crystallization sequences of LS and US were the result of polybaric fractionation of magma batches having a similar initial composition and considered, therefore, LS and US as cogenetic and coeval. Girardi et al. (1986) also observed an upward increase of hydrous phases (amphibole and minor biotite) in LGZ and the widespread presence of amphibole in US and proposed that this was a consequence of an increase of water in the residual melt. These authors and Fornoni Candia et al. (1989) described in detail the subsolidus mineral reactions, which did not blur the original cumulus textures, and hypothesized they were the result of re-equilibration under isobaric slow cooling conditions.

The cited stratigraphy is accepted by most Niquelândia students, although different names have often been used for indicating the various stratigraphic units. A major debate concerns the interpretation of the subsolidus mineral assemblages and the cogenesis of US and LS. Based on the observation that the LS and US mineral assemblages formally represent the expected result of mafic-rock re-equilibration under granulite and amphibolite facies conditions, respectively, various authors inferred that granulite and amphibolite facies metamorphic events affected Niquelândia during the Proterozoic (e.g. Ferreira Filho, 1998 and references therein). The latter authors also inferred a metamorphic event transitional between granulite and amphibolite facies in a belt corresponding with the upper LGZ – lower UGAZ regions (the "hydrous zone").

Ages considered as metamorphic span from 610 Ma (Ferreira Filho et al., 1994; Ferreira Filho and Pimentel, 2000) to 760–790 Ma (Pimentel et al., 2006 and references therein).

The ages estimated for the crystallization of the complex span from 2 Ga to 0.8 Ga (Ferreira Filho et al., 1994; Correia et al., 1996, 1999; Ferreira Filho and Pimentel, 2000; Pimentel et al., 2004). Based on zircon U–Pb data, Pimentel et al. (2004) argued that LS is Neoproterozoic (797 ± 10 Ma) whereas US is Mesoproterozoic (1248 ± 23Ma). On this basis, they inferred that LS and US are two distinct, tectonically juxtaposed layered complexes. Pimentel et al. (2006) presented further zircon ages supporting crystallization of LS at ~800 Ma. Correia et al. (2006) provided dating of igneous zircon occurring in anorthosite layers of US, resulting in 833 ± 21 Ma. Therefore, at present there is a convergence of zircon data indicating Neoproterozoic intrusion of LS but a large divergence for the intrusion age of US. The age of 1248 ± 23 Ma derives from zircon cores of sample CF-04, a mylonite occurring in a shear zone into gabbros close to the US base. CF-04 is constituted by quartz, garnet, accessory plagioclase, kyanite and zircon (Pimentel et al., 2004). Zircon core analyses

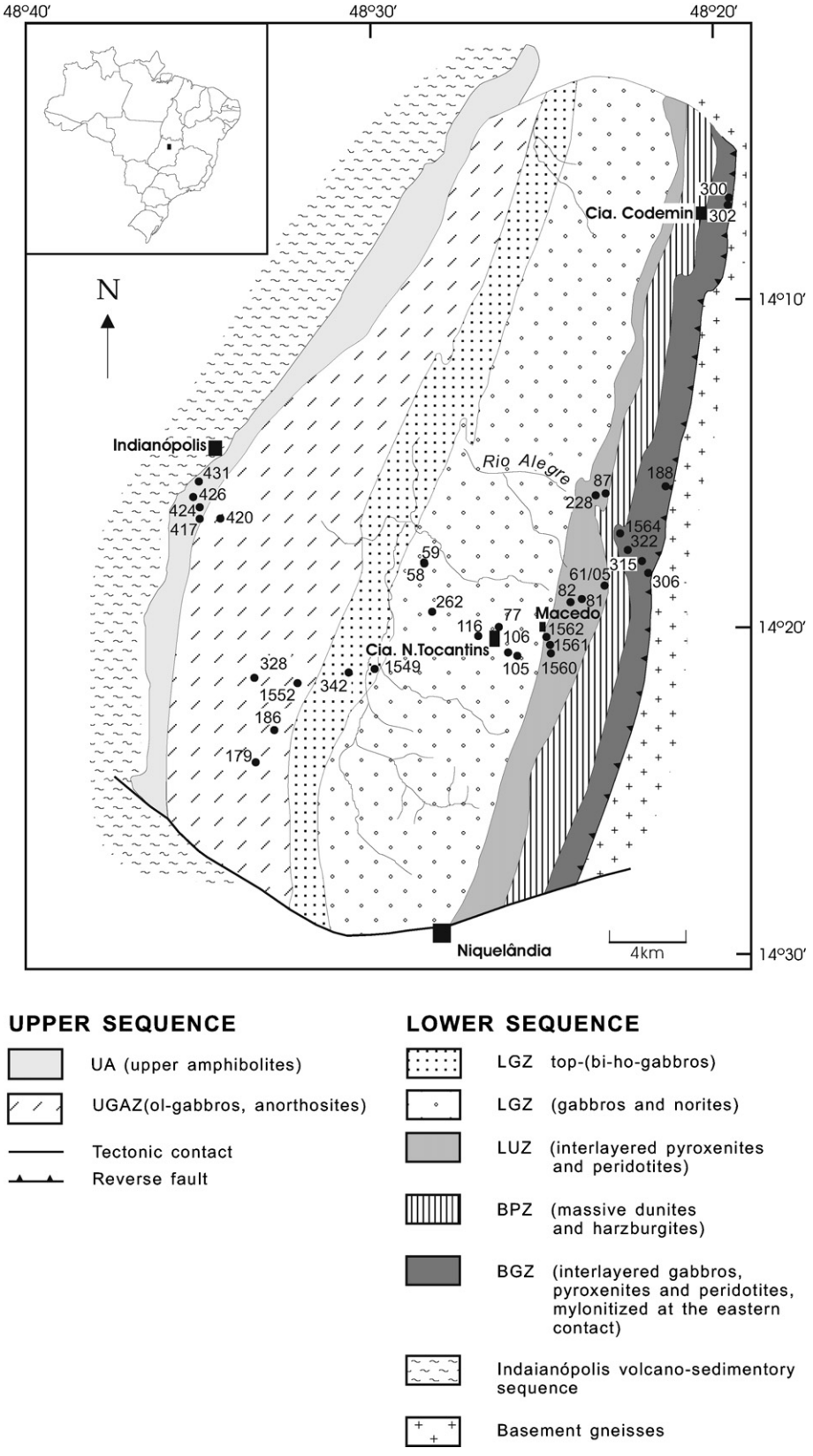

Fig. 1. Sketch geological map of the Niquelândia complex (Girardi et al., 1986) and sample location.

fall along a poorly constrained discordia line between 0.76 and 1.25 Ga. The upper intercept, constrained by the $^{207}Pb/^{206}Pb$ ages of four analyses, is 1248 ± 23Ma, assumed to be the age of crystallization. However, the mineral assemblage of sample CF-04 indicates that it is not likely to derive from an igneous protolith, but rather

it represents a metasedimentary rock, possibly derived from the country rocks of the complex.

On the other hand, the zircons analysed by Correia et al. (2006) in an US anorthosite do not have inherited cores, most of them are prismatic and have high Th/U ratios, thus supporting their igneous origin and Cryogenian Neoproteroic ages for the igneous crystallization of the complex.

As evident, isotopic data available at present do not provide definite support neither for the hypothesis that LS and US are intrusions of different ages, nor for the possibility that they are coeval. However, this latter possibility seems to us more probable on the basis of the age determinations on zircons by Pimentel et al. (2006) for LS and Correia et al. (2006) for US. Therefore, we adopt the hypothesis that LS and US are coeval and record a crystallization age at 830 Ma. Reasonable different assumptions on the age (eg., 830 Ma ± 30) would not alter neither the isotopic arrays shown in Fig. 2 nor our modelling.

3. Analytical methods

Bulk rock major element analyses were performed at the X-ray fluorescence laboratory at the Departamento de Mineralogia e Geotectônica, Instituto de Geociências, University of São Paulo (GMG-IGc-USP), Brazil, by wavelength dispersive X-ray spectrometer (Philips PW 2400) using fused glass discs according to the procedures described in Mori et al. (1999). In order to avoid potential contaminations from steel and tungsten carbide crushing equipment, all whole rock powders for XRF analysis were prepared using a hydraulic press for crushing, an agate mill and a vibratory agate micronizer to prepare the sample powders. Limits of detection are of the order of 1–10 ppm. The precisions are better than 2%. The analyses were carried out by comparison with the international standards JB1a e JG1a.

REE in bulk-rock powders were analysed by Inductively Coupled Plasma - Mass Spectrometry (ICP-MS) at the Laboratorio de Quimica e ICP, GMG-IGc-USP. Samples were dissolved in Parr bombs in a microwave furnace as described by Navarro (2004). Accuracy, determined with respect to the reference standards BHVO-2 and BR, is 0.5–2%.

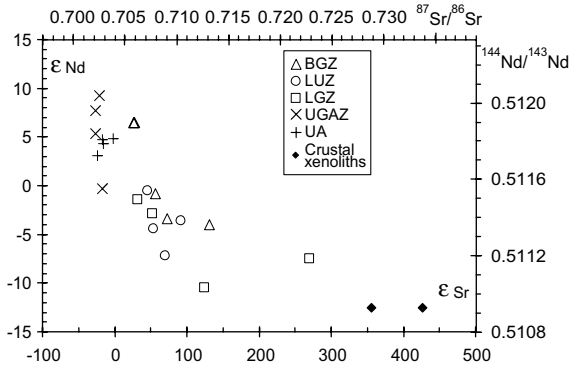

Fig. 2. $\varepsilon Sr_{830\ Ma}$–$\varepsilon Nd_{830\ Ma}$ isotopic array for the LS and US selected rocks.

Isotopic analyses in bulk-rock were carried out at Geochronological Research Center (CPGeo-USP). The Rb–Sr and Sm–Nd analyses were prepared by standard methods described by Sato et al. (1995). Abundances of Rb and Sr were determined by isotope dilution using ^{87}Rb and ^{84}Sr enriched spikes. Each sample was ultrasonically washed in triple distilled water before chemical attack and all samples were totally digested with $HF_{(conc.)}$ plus $HNO_{3(conc.)}$ in a proportion 2:1, using Parr type bombs. The solutes were evaporated to dryness and converted to chloride form with 2.62 N HCl. Sr was separated in AG 50 WX8, 200–400 mesh cationic resin, loaded on Ta filaments together with 2μl H_3PO_4 and analysed in the 262 Finnigan-Mat mass spectrometer. The Sr isotopic ratios were normalized to $^{86}Sr/^{88}Sr = 0.1194$; replicate analyses of $^{87}Sr/^{86}Sr$ for the NBS987 standard gave a mean value of 0.71028 ± 0.00006 (2σ). Concentration of Sr in the blanks were less than 5 ng.

Samples for Sm–Nd analyses were spiked with a ^{150}Nd–^{149}Sm spike and dissolved with $HF_{(conc.)}$ and $HNO_{3(conc.)}$ in proportion 2:1, also in Parr type bombs. The solutes were evaporated, dissolved with 0.2 ml 2.5 N HCl and the rare earth elements (REE) were separated with 6.2 N HCl in a AG 50WX8, 200–400 mesh cationic exchange resin. The solutions were dried and re-dissolved in 0.26 N HCl and Sm was collected with 0.55 N HCl. Both elements were loaded as phosphates on Re filaments and analysed in the 262 Finnigan-Mat mass spectrometer. Measurements of $^{143}Nd/^{144}Nd$ were normalized to $^{146}Nd/^{144}Nd = 0.719$. The averages of $^{143}Nd/^{144}Nd$ for La Jolla and BCR-1 standards were 0.511847 ± 0.00005 (2σ) and 0.512662 ± 0.00005 (2σ), respectively. Concentrations of Nd in the blanks were less than 0.03 ng.

4. Selected samples

The locality of the samples selected for this study is shown in Fig. 1 and their major element composition and REE concentration are reported in Table 1, along with information on their mode. Except for one anorthosite (Niq 1552) and one amphibolite (Niq 420), the samples from all the stratigraphic units up to UGAZ are gabbroic rocks. Most of them are gabbronorites. Amphibolites represent UA. Gabbroic rocks were preferred because they represent either the crystallization result of a melt close to a polisaturated temperature minimum point or mixtures of cumulus crystals and residual, interstitial melt. In both cases they may better record open-system processes concomitant with crystallization. Another reason is that these rocks have higher incompatible trace element concentrations with respect to cumulus pyroxenites and peridotites, thus decreasing the error in the analytical determinations.

In most LS samples subsolidus effects are manifested only by unmixing lamellae in pyroxenes. The BGZ

Table 1
Major (wt%) and REE (ppm) concentrations and modal composition of the rocks considered in this study

Sample	X-ray fluorescence analyses in wt%											
	SiO_2	TiO_2	Al_2O_3	FeO_t	MnO	MgO	CaO	Na_2O	K_2O	P_2O_5	L.O.I.	Tot
BGZ												
Niq188	49.17	0.15	19.55	4.53	0.12	9.85	14.84	1.14	0.02	0.01	0.12	99.50
Ni300	50.21	0.19	14.22	7.00	0.15	11.85	11.67	1.68	0.12	0.04	2.10	99.23
Niq306	48.67	0.76	15.09	9.08	0.15	9.63	11.15	1.54	0.16	0.06	2.70	98.99
Niq315	49.44	0.16	17.66	4.28	0.11	12.05	13.98	1.04	0.02	0.06	0.75	99.55
Niq322	49.29	0.16	18.47	7.30	0.14	9.37	11.71	0.93	0.07	0.05	1.70	99.19
NQ1564	49.70	0.12	13.84	5.82	0.12	15.09	12.81	0.94	0.06		0.46	98.96
LUZ												
Niq81	50.27	0.08	20.36	6.21	0.12	8.16	11.94	2.08	0.07	0.01		99.29
Niq82	47.60	0.08	23.31	3.19	0.06	9.69	13.54	1.24	0.03	0.003	0.22	98.97
Niq87	50.37	0.13	17.52	6.04	0.13	10.51	12.49	1.38	0.07	0.003	0.08	98.71
Niq228	50.87	0.17	15.06	7.09	0.15	10.87	12.57	1.57	0.06	0.003	0.30	98.71
Nq 1560/95	50.01	0.28	15.16	8.42	0.18	10.04	14.08	1.50	0.04		0.25	99.96
NQ1561/95	50.16	0.21	15.30	12.93	0.22	11.32	8.91	1.19	0.05			100.29
NQ1562/95	48.92	0.11	17.91	10.33	0.21	11.38	10.66	0.71	0.02			100.25
NIQ-61/05	49.71	0.17	14.66	7.23	0.15	14.71	11.13	0.84	0.29	0.005	0.08	98.98
LGZ												
Niq77	49.38	0.71	18.31	9.29	0.15	7.22	11.95	1.77	0.16	0.04	0.04	99.02
Niq105	47.88	0.97	17.90	12.76	0.80	6.41	10.44	1.95	0.10	0.02		99.23
Niq106	49.05	0.41	19.86	9.72	0.15	6.11	11.48	2.02	0.12	0.02		98.94
Niq116	49.54	0.18	20.64	5.52	0.12	8.77	12.98	1.40	0.06	0.02	0.18	99.41
Niq262	46.86	0.70	20.18	9.16	0.17	7.71	13.13	1.03	0.04	0.01		98.99
Niq342	48.42	0.94	15.41	12.12	0.21	11.54	6.32	1.00	1.48	0.31	0.92	98.67
NQ1549/95	51.66	0.95	13.95	12.57	0.22	12.06	6.25	1.18	0.99	0.17		100.00
UGAZ												
Niq179	50.12	0.54	16.68	8.99	0.18	8.59	11.86	2.03	0.12	0.01	0.57	99.69
Niq186	47.19	0.36	15.20	8.52	0.17	12.15	14.13	1.30	0.04	0.01	0.38	99.45
Niq328	45.99	0.74	16.81	11.43	0.23	8.96	12.80	1.79	0.08	0.04	0.86	99.73
Niq420	55.07	1.98	12.98	11.08	0.15	4.29	8.11	3.78	0.06	0.60	1.00	99.10
NQ1552	46.66	0.05	33.63	0.70	0.01	0.20	14.86	2.61	0.04	0.004	0.28	99.04
UA												
Niq417	47.62	1.93	12.79	14.96	0.21	6.87	10.63	2.46	0.29	0.23	0.60	98.59
Niq424	45.17	2.71	13.90	14.47	0.20	7.40	10.38	2.37	0.56	0.36	0.53	98.05
Niq426	45.27	1.24	13.82	12.69	0.22	9.78	12.22	1.87	0.34	0.13	0.73	98.31
Niq431	47.97	1.48	12.73	12.72	0.19	7.63	12.15	2.34	0.22	0.16	0.69	98.28
Crust												
Niq58/05	63.98	0.93	19.90	8.81	0.04	1.79	0.09	0.42	3.37	0.05	0.44	99.82
Niq59/05	63.15	0.93	21.04	9.93	0.04	1.15	0.05	0.43	3.47	0.04	0.36	100.59

ICP-MS analyses in ppm

	La	Ce	Pr	Nd	Sm	Eu	Gd	Tb	Dy	Ho	Er	Tm	Yb	Lu
BGZ														
Niq188	0.10	0.37	0.08	0.54	0.29	0.20	0.52	0.11	0.77	0.19	0.54	0.09	0.56	0.08
Ni300	1.33	2.25	0.28	1.30	0.40	0.33	0.54	0.10	0.73	0.18	0.51	0.08	0.53	0.08
Niq306	1.93	5.50	0.82	4.43	1.52	0.68	1.91	0.38	2.62	0.61	1.72	0.26	1.79	0.26
Niq315	0.40	0.99	0.16	0.92	0.36	0.18	0.54	0.10	0.73	0.18	0.50	0.08	0.51	0.07
Niq322	0.39	0.96	0.15	0.84	0.32	0.27	0.42	0.09	0.66	0.17	0.48	0.08	0.53	0.08
NQ1564	0.34	0.97	0.15	0.87	0.30	0.16	0.35	0.08	0.60	0.15	0.45	0.07	0.50	0.08
LUZ														
Niq81	0.11	1.35	0.02	0.16	0.07	0.16	0.17	0.04	0.29	0.08	0.24	0.04	0.28	0.05
Niq82	0.40	0.86	0.11	0.55	0.17	0.19	0.21	0.04	0.26	0.06	0.18	0.03	0.18	0.04
Niq87	0.44	1.12	0.16	0.81	0.28	0.26	0.46	0.08	0.53	0.13	0.38	0.06	0.42	0.06
Niq228	0.11	0.92	0.06	0.46	0.29	0.29	0.59	0.12	0.88	0.22	0.65	0.11	0.69	0.11
Nq 1560/95	1.03	2.59	0.41	2.30	0.80	0.42	0.85	0.18	1.19	0.28	0.76	0.12	0.74	0.11
NQ1561/95	0.38	0.70	0.09	0.52	0.19	0.47	0.23	0.06	0.46	0.13	0.41	0.07	0.57	0.10
NQ1562/95	0.45	0.72	0.10	0.47	0.13	0.42	0.14	0.03	0.24	0.06	0.19	0.03	0.27	0.04
NIQ-61/05	0.70	0.60	0.60	0.90	1.20	2.40	1.60	1.40	1.90	1.90	2.10	1.70	2.00	1.60
LGZ														
Niq77	2.46	5.98	0.91	4.81	1.64	0.73	2.78	0.46	2.82	0.66	1.88	0.30	1.91	0.29
Niq105	0.53	1.54	0.33	2.36	1.19	1.07	2.16	0.42	2.66	0.65	1.85	0.31	2.04	0.30
Niq106	2.58	5.28	0.51	2.32	0.69	0.54	0.98	0.19	1.24	0.34	0.97	0.16	1.25	0.18
Niq116	1.13	2.76	0.34	1.63	0.51	0.31	0.83	0.13	0.87	0.21	0.60	0.10	0.62	0.10
Niq262	1.54	3.88	0.45	2.02	0.53	0.49	0.65	0.11	0.65	0.15	0.43	0.07	0.47	0.07
Niq342	22.03	46.86	6.17	26.50	5.44	1.50	4.21	0.75	4.28	0.93	2.64	0.41	2.69	0.41
NQ1549/95	14.53	29.72	3.82	16.53	3.58	1.37	3.17	0.56	3.30	0.73	2.11	0.34	2.22	0.36
UGAZ														
Niq179	0.69	1.62	0.26	1.49	0.62	0.43	0.96	0.18	1.20	0.28	0.77	0.12	0.78	0.12
Niq186	1.03	2.85	0.45	2.47	0.92	0.40	1.25	0.24	1.56	0.36	0.98	0.15	0.92	0.14
Niq328	0.31	0.95	0.19	1.27	0.60	0.35	0.93	0.18	1.17	0.28	0.74	0.12	0.72	0.11
Niq420	33.46	69.94	10.06	44.56	11.66	2.24	14.04	2.29	13.72	3.17	8.46	1.30	7.72	1.14
NQ1552	0.44	0.95	0.13	0.59	0.14	0.29	0.12	0.02	0.11	0.02	0.06	<0.01	0.05	<0.01
UA														
Niq417	6.00	15.10	2.46	12.58	3.95	1.30	5.06	0.89	5.45	1.28	3.45	0.55	3.36	0.51
Niq424	14.08	34.51	5.05	23.35	5.96	1.87	6.64	1.02	5.93	1.28	3.38	0.51	3.09	0.46
Niq426	3.45	9.49	1.49	7.66	2.43	0.84	3.17	0.56	3.46	0.83	2.24	0.36	2.22	0.33
Niq431	4.60	11.90	1.89	9.62	3.09	1.04	4.02	0.71	4.40	1.03	2.78	0.44	2.73	0.41
Crust														
Niq58/05	34.30	79.43	7.95	28.20	4.51	1.11	3.71	0.42	2.13	0.35	0.95	0.10	0.70	0.10
Niq59/05	15.93	39.78	2.85	9.85	1.33	0.48	1.20	0.09	0.42	0.05	0.15	<0.01	0.08	0.01

(*continued on next page*)

Table 1 (*continued*)

	Modal composition in volume % *										Others
	Plag	Cpx	Opx	Ol	Qtz	KF	Gr	Sill	Amph	Bt	
BGZ											
Niq188	53	27	19								1 Op
Ni300	41	29	28								1 Chl, 1 Ep
Niq306	43	23	29								3 Op, 1 Chl, 1 Ep
Niq315	45	30	24								1 Op
Niq322	49	19	30								2 Op
NQ1564	35	50	14								1 Op
LUZ											
Niq81	61	15	23								1 Op
Niq82	63	13	23								1 Op
Niq87	49	23	28								tr Op
Niq228	42	31	26								1 Op
Nq 1560/95	55	40	5								tr Op
NQ1561/95	50	24	25								1 Op
NQ1562/95	50	10	40								tr Op
NIQ-61/05	45	25	30							tr	tr Op
LGZ											
Niq77	54	15	30								1 Op
Niq105	52	15	29								4 Op
Niq106	55	15	25								2 Op, 3 Qtz
Niq116	57	16	26								1 Op
Niq262	55	16	26								3 Op
Niq342	45	7	30						4	10	2 Op, 2 Qtz
NQ1549/95	46	8	39							7	tr Ru, tr Zr
UGAZ											
Niq179	46	19	12						20		3 Op
Niq186	35	30	10	4					2		2 Op, 17 Kel
Niq328	47	26	19								2 Op, 6 Kel
Niq420	40		14						40		1 Gr, 2 Op, 3 Qtz
NQ1552	90								6		3 Ep, 1 Sca, tr Zr
UA											
Niq417	28	20	15						35		1 Op, 1 Qtz
Niq424	25	1	5						61		4 Op, 4 Qtz
Niq426	25								71		2 Op, 2 Sph
Niq431	32								64		2 Op, 2 Sph
Crust											
Niq58/05					40	26	16	11		7	Op Tr Sp
Niq59/05					34	31	16	14		1	4 Op

*: Plag, plagioclase; Cpx, clinopyroxene; Opx, orthopyroxene; Ol, olivine; Amph, amphibole; Bt, biotite; Op, opaques; Ep, epidote; Zr, zircon, Chl, chlorite; Ap, apatite; Gr, garnet; Qtz, quartz; Sca, scapolite; Sph, sphene; Kfs, K feldspar, Sill, sillimanite; Sp, spinel; Kel, keliphite (Opx + Cpx + Spinel ± Amph ± Grt); tr = trace content.

samples, however, show evidence of strong deformation, recrystallization and in samples Niq300 and Niq306 partial alteration of plagioclase and pyroxenes into chlorite and epidote. These effects are induced by the fault system limiting the lower border of the complex. In the US samples, subsolidus re-equilibration is documented by coronitic textures described in detail by Fornoni Candia et al. (1989). The selected samples do not show evidence of important trace element mobility during post-magmatic recrystallization, as discussed in detail by Girardi et al. (1986).

In addition, two sillimanite–garnet–biotite gneisses, occurring as xenoliths close to the LGZ top, have also been analysed because they may be indicators of the composition of the contaminant.

5. Sr and Nd isotopes

The isotopic values of the selected samples are shown in Table 2 and illustrated in Fig. 2. εSr and εNd have been recalculated at 830 Ma, assumed to represent the possible age of emplacement of the complex.

All the US rocks have positive εNd and slightly negative εSr, except sample Niq 420, whose εNd is close to zero. All the LS samples have negative €Nd and positive €Sr values, except the BGZ gabbronorites Niq 188 and Niq 1564 (see Table 2), whose εNd are 6.5 and 2.2 respectively. The crustal xenoliths have very high εSr (exceeding 300) and very negative εNd (−12.5).

The Niquelândia gabbroic rocks describe an array between the isotopically depleted region (DM) and an isotopically enriched region occupied by the crustal xenoliths. The general configuration of the array indicates that the first melts originated from a depleted mantle source, which is in accordance with isotopic and geochemical studies performed in LUZ chromitites (Girardi et al., 2006). More in detail, both the US units form an array characterized by comparatively large εNd_{830} variations and virtually constant $€Sr_{830}$ at <0 values. In LS, the various units form an array where the Nd and Sr isotopic values decrease and increase, respectively, from BGZ to LUZ and LGZ. This array points towards the isotopically enriched crustal end-member. Much of the spread observed in the LS is caused by distinct sub-arrays of its various units.

6. Rare earth elements

REE concentrations are reported in Table 1. Fig. 3 illustrates the REE profiles of the selected samples normalized to Primitive Mantle (PM, Hofmann, 1988). The REE concentration of LGZ and of the US units is on average much higher than that found in BGZ and LUZ. Within each unit, there is a large concentration range and a large variation of the REE profiles, from LREE-depleted to virtually flat, to LREE-enriched. In most samples, the normalized REE concentration remains virtually constant from Sm to Yb both in LREE-depleted and LREE-enriched rocks. Most LREE-enriched and depleted rocks exhibit a positive Eu anomaly (except in UA), indicating enrichment in cumulus plagioclase. The positive Eu anomaly fades out with increasing REE concentration and may even become negative (e.g., Niq 420 in UGAZ).

The REE fractionation and LREE enrichment (e.g. La_n/Sm_n, since the pattern is flat from Sm to Yb) is accompanied in LS by a decrease of $€Nd_{830}$ and increase of $€Sr_{830}$ and in US only by the εNd variation. This can be seen by comparing the isotope data in Table 2 with Fig. 2 and will be graphically illustrated later, in Section 7.2.

7. Discussion

The large isotopic variations of the Niquelândia gabbros cannot be explained either by any closed system magmatic process, including mixing of cumulates and residual melts, which could induce variations of the geochemical parameters, but not of isotopes, or by post magmatic re-equilibration or high-temperature metamorphism. They strongly favour contamination. Modelling of the contamination process requires preliminary information on the composition of the parent magma and of the contaminant. An estimate of the first is reported in Girardi et al. (1986), who proposed that the Niquelândia parent magma was a picritic basalt. As for the second, contaminants could have been the rocks of the Paleoproterozoic basement or those of the Proterozoic Indaianópolis sequence, both older than the estimated age of the complex. Because of heavy cover and alteration, reliable analytical data on the composition of the Paleoproterozoic basement are impossible to obtain. Data on the Indaianópolis volcano-sedimentary sequence are not available in the Niquelândia region but only in other correlated areas, the nearest of which is Barro Alto (Fuck et al., 1989; Moraes et al., 2003, 2006) and anyway the analyses reported in the quoted papers do not have Sr and Nd isotope determinations on the same sample. Therefore, we have adopted the metapelitic xenoliths occurring at the LGZ top as representative contaminants. This is probably an oversimplification and does not warrant against the possibility that more than one contaminant affected the complex. Anyway, any melt derived from crustal rocks would have high Sr - low Nd isotopic values and would be LREE enriched (see the compositions of various crustal types in Taylor and McLennan, 1985), like the analysed xenoliths.

7.1. Modelling

Open system processes where magmas become contaminated by the crust are traditionally modelled by means of an AFC (Assimilation-Fractional Crystallization) approach (DePaolo, 1981), where the heat released by crystallization induces melting of the country rock and the residual magma is thereby contaminated. Traditional AFC modelling, however, is too simplistic in that it conserves species and mass, but it neglects energy, i.e. the relationship between the temperature of the magma and

Table 2
Sr and Nd isotopic composition of the rocks reported in Table 1

Sample	Rb	Sr	$^{87}Rb/^{86}Sr$	Error	$^{87}Sr/^{86}Sr$	Error	Sm	Nd	$^{147}Sm/^{144}Nd$	Error	$^{143}Nd/^{144}Nd$	Error	Sr 830 Ma	Nd 830 Ma	εSr 830 Ma	εNd 830 Ma
BGZ																
Niq188	0.59	58.67	0.0293	0.0002	0.70650	0.00002	0.312	0.560	0.3364	0.0011	0.513730	0.000010	0.70615	0.511899	26.08	6.48
Ni300	2.43	128.28	0.0549	0.0004	0.71423	0.00002	0.383	1.214	0.1906	0.0006	0.512402	0.000016	0.71358	0.511365	131.60	−3.96
Niq306	0.39	52.38	0.0213	0.0002	0.70971	0.00004	1.547	4.336	0.2157	0.0007	0.512567	0.000012	0.70946	0.511393	73.11	−3.40
Niq315	0.34	56.37	0.0176	0.0001	0.70850	0.00004	0.366	0.898	0.2466	0.0009	0.512865	0.000019	0.70829	0.511523	56.47	−0.87
Niq322							0.288	0.728	0.2394	0.0008	0.512564	0.000013		0.511261		−5.99
NQ1564							0.302	0.862	0.2130	0.0004	0.512840	0.000042		0.511681		2.22
LUZ																
Niq81	0.75	90.58	0.0241	0.0002	0.70955	0.00002	0.078	0.168	0.2807	0.0011	0.512729	0.000644	0.70926	0.511201	70.33	−7.16
Niq82							0.167	0.524	0.1928	0.0008	0.512063	0.000406		0.511014		−10.83
Niq87	0.36	99.85	0.0104	0.0001	0.71091	0.00002	0.305	0.928	0.1986	0.0007	0.512466	0.000013	0.71079	0.511385	91.95	−3.56
Niq228	0.92	93.30	0.0286	0.0002	0.70843	0.00002	0.300	0.479	0.3790	0.0013	0.513405	0.000012	0.70809	0.511343	53.72	−4.39
NQ1560/95							0.521	1.417	0.2238	0.0001	0.512752	0.000026		0.511534		−0.65
NQ1561/95							0.149	0.389	0.2323	0.0001	0.512585	0.000028		0.511320		−4.83
NQ1562/95							0.089	0.286	0.1883	0.0002	0.512324	0.000021		0.511299		−5.24
NIQ-61/05	0.44	86.61	0.0145	0.0001	0.70774	0.00004			0.2970		0.513160		0.70757	0.511543	46.25	−0.47
LGZ																
Niq77	0.29	71.63	0.0116	0.0001	0.70674	0.00002	1.700	4.821	0.2133	0.0007	0.512656	0.000011	0.70660	0.511495	32.49	−1.42
Niq105	0.12	109.28	0.0033	0.0000	0.70804	0.00002	1.210	2.334	0.3135	0.0010	0.513127	0.000012	0.70800	0.511421	52.39	−2.87
Niq106	0.46	84.19	0.0159	0.0001	0.71331	0.00004	0.734	2.372	0.1871	0.0006	0.512049	0.000011	0.71312	0.511030	125.15	−10.50
Niq116							0.469	1.478	0.1918	0.0006	0.512444	0.000016		0.511400		−3.27
Niq262							0.481	1.737	0.1676	0.0006	0.512074	0.000011		0.511162		−7.93
Niq342	61.33	203.38	0.8750	0.0018	0.73366	0.00002	5.390	25.665	0.1270	0.0005	0.511874	0.000011	0.72328	0.511183	269.40	−7.52
NQ1549/95							3.255	15.279	0.1296	0.0001	0.511982	0.000023		0.511276		−5.69
UGAZ																
Niq179	2.00	151.08	0.0383	0.0003	0.70285	0.00003	0.609	1.459	0.2523	0.0009	0.513333	0.000011	0.70240	0.511960	−27.18	7.67
Niq186	0.45	87.42	0.0150	0.0001	0.70262	0.00002	0.933	2.453	0.2300	0.0040	0.513094	0.000010	0.70244	0.511842	−26.58	5.38
Niq328	0.94	125.42	0.0217	0.0002	0.70308	0.00002	0.610	1.274	0.2895	0.0010	0.513618	0.000012	0.70283	0.512043	−21.07	9.29
Niq420	1.23	157.73	0.0225	0.0002	0.70339	0.00001	12.088	44.921	0.1627	0.0006	0.512439	0.000010	0.70312	0.511554	−16.91	−0.27
NQ1552							0.118	0.521	0.1373	0.0001	0.512506	0.000029		0.511758		3.74
UA																
Niq417	9.84	122.14	0.2332	0.0018	0.70583	0.00002	4.125	12.696	0.1965	0.0007	0.512881	0.000010	0.70307	0.511812	−17.65	4.77
Niq424	8.23	238.98	0.0997	0.0008	0.70386	0.00001	5.983	22.655	0.1597	0.0005	0.512596	0.000011	0.70268	0.511727	−23.16	3.12
Niq426	8.44	126.58	0.1929	0.0015	0.70647	0.00005	2.398	7.290	0.1989	0.0007	0.512898	0.000012	0.70418	0.511815	−1.81	4.85
Niq431	4.35	110.15	0.1142	0.0009	0.70452	0.00003	3.178	9.628	0.1996	0.0007	0.512872	0.000010	0.70317	0.511786	−16.19	4.26
Crust																
Niq58/05	80.10	102.70	2.2700	0.0560	0.75625	0.00007	5.851	35.373	0.1000	0.0003	0.511469	0.000008	0.72934	0.510925	355.34	−12.56
Niq59/05	58.90	127.60	1.3410	0.0310	0.75029	0.00002	3.014	21.070	0.0865	0.0003	0.511396	0.000012	0.73439	0.510925	427.14	−12.55

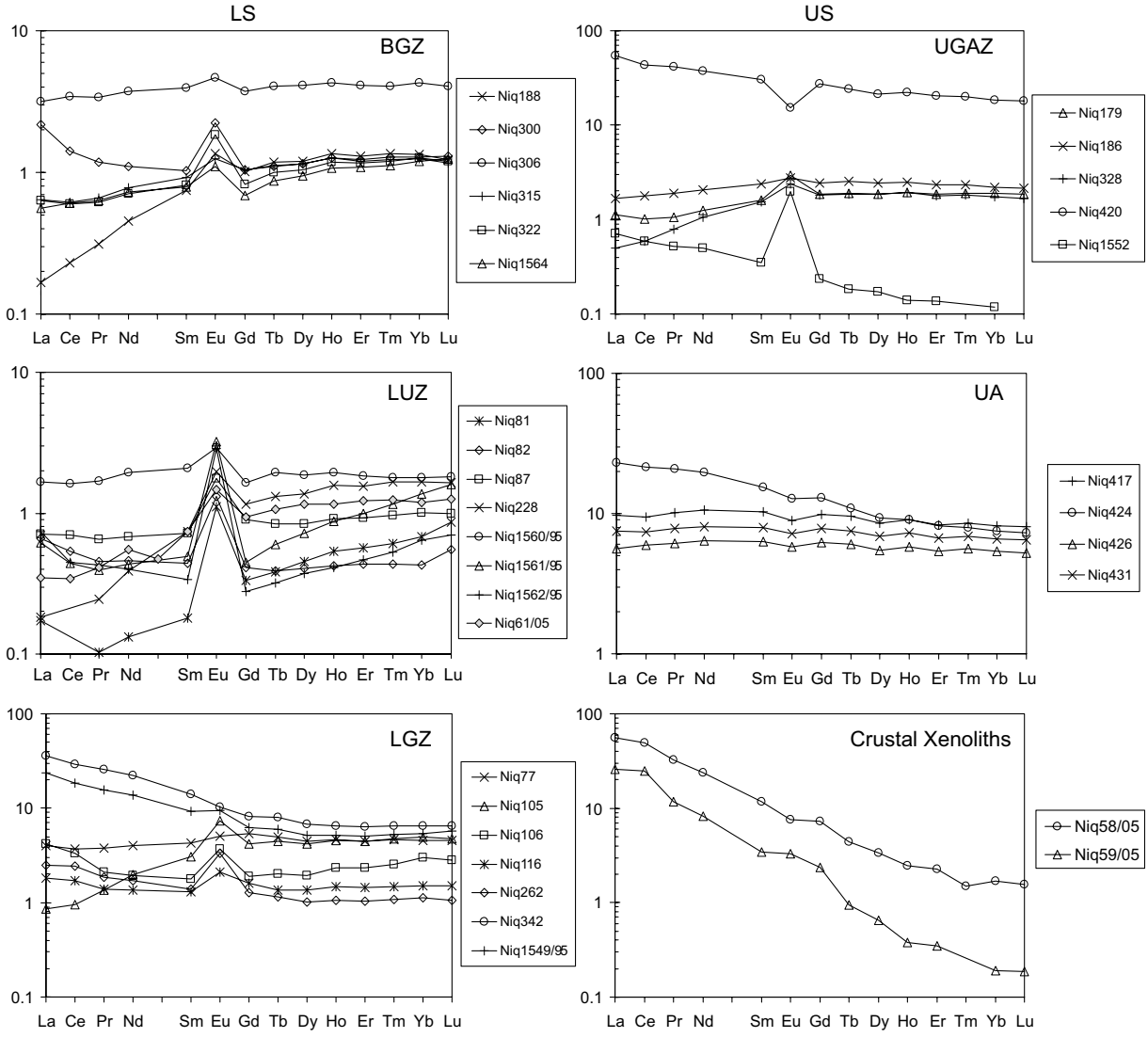

Fig. 3. REE patterns of selected samples, normalized to Primitive Mantle (Hofmann, 1988). Note the different scale in BGZ and LUZ with respect to the other units.

of the crust and the heat to be released from the magma in order to warm the crust to its melting temperature. Spera and Bohrson (2001), provided an Energy Constrained, Assimilation Fractional Crystallization model (EC-AFC) which takes into account the energy involved and Bohrson and Spera (2001) document with various examples how this more rigorous model may lead to different results and interpretations with respect to a traditional AFC approach. Therefore, we have used the EC-AFC approach in order to model the isotopic variation trends at Niquelândia. The acronyms of the input parameters are from Spera and Bohrson (2001). Input data used for Niquelândia are reported in Table 3A and 3B and are hereafter specified.

The heat of crystallization (Hcry) and heat of fusion (Hfus) were taken from Spera and Bohrson (2001).

The liquidus temperature of the magma (Tl_m) has been inferred by using the MELTS program (Ghiorso and Sack, 1995; Asimow and Ghiorso, 1998) applied to the composition estimated for the parent Niquelândia magma (Girardi et al., 1986) at FMQ oxygen fugacity and 0.1 GPa. It results 1360 °C.

The initial temperature of the magma (Tm_o) at intrusion is arbitrarely assumed to be 1250 °C.

The initial temperature of the wallrock (Ta_o) has been assumed as 700 °C. The rationale for this relatively high temperature is that igneous intrusions are generally preceded by thermal heating of the intrusion region. The effect of using lower Ta_o would be that more energy would be spent by heating wallrocks to their melting point, thus shortening the assimilation range. The liquidus temperature of the assimilated material (Tl_a) has been assumed to be 1250 °C.

The solidus temperature (T_s), required to be the same for magma and assimilated material, has been fixed at 850 °C, which is close to the solidus temperature of pelitic rocks under vapour-absent conditions (Vielzeuf and Holloway, 1988) and to the final solidus temperature in hydrous igneous residues.

Table 3
Input parameters used for modelling the LS (A) and US (B) variations

A								
T_{lm}	1360 °C		Sr	Nd	La	Sm	$^{87}Sr/^{86}Sr$	$^{143}Nd/^{144}Nd$
T_{m0}	1250 °C	Magma	50	4.94	1.72	1.66	0.7024	0.51196
T_{la}	1250 °C	Bulk D_0	0.4	0.25	0.06	0.38		
T_{a0}	700 °C	Contaminant	100	38	64	11.4	0.7319	0.51092
T_s	850 °C	Bulk D_0	0.69	0.4	0.27	1.3		
B								
T_{lm}	1360 °C	Element	Sr	Nd	La	Sm	$^{87}Sr/^{86}Sr$	$^{143}Nd/^{144}Nd$
T_{m0}	1250 °C	Magma	50	4.94	1.72	1.66	0.7024	0.51196
T_{la}	1250 °C	Bulk D_0	0.4	0.25	0.06	0.38		
T_{a0}	700 °C	Contaminant	100	38	64	11.4	0.7319	0.51092
T_s	850 °C	Bulk D_0	2	0.11	0.13	0.14		

Trace element concentrations are in ppm. Symbols are explained in the text.

The final temperature to which the magma cools and wall rock heats up (T_{eq}) has been fixed arbitrarily at 950 °C for LS and 850 °C for US. These different values are based on the much larger volume of LS with respect to US, which should correspond to a larger heat production.

Isotope composition of the magma has been assumed equal to that of sample Niq 179, which has the lowest isotopic Sr value. Trace element composition of the initial magma has been assumed to be that of a picritic basalt having 0.45 × N-MORB trace element concentrations, in agreement with Girardi et al. (1986). That of the wall rock has been assumed as the average composition of the two crustal xenoliths both for isotopes and trace elements.

The bulk partition coefficients for the magma were estimated assuming the following average modal proportions: 40% (Ol + Opx), 40% Cpx, 20% Pl both for LS and US. REE partition coefficients were taken from Henderson (1984) and Greeen (1994). Partition coefficients for Sr in plagioclase have been estimated from plagioclase composition using the equations of Blundy and Wood (1991) and Bindeman et al. (1998). $^{Pl}D_{Sr}$ ranges from 1.4 to 1.6 in BGZ and LUZ, 1.8–2.4 in LGZ and 1.8–4.9 in UGAZ. D_{Sr} for Ol, Opx and Cpx were estimated from Greeen (1994).

Partition coefficients for the crustal component need some specifications. Ferreira Filho et al. (1998) found that metasedimentary lithotypes in the amphibolite facies region (our US) were characterized by Pl, Qtz, Sil, Bi ±Kfs, whereas in the granulite facies (our LS), mineral assemblages such as spinel + quartz and garnet + sillimanite + quartz occur. According to Vielzeuf and Holloway (1988) and Patiño Douce and Jonhston (1991) dehydration melting of a pelite (such as that represented in the xenoliths) has a large melt productivity in the range 850° – 875 °C by reaction of the type: Bi + Als + Pl + Qtz = L + Gr (±Kfs). Plagioclase disappears at about 900 °C and the high T refractory residue consists of garnet and Als and of Sp + Qtz at temperature above 1050 °C. Thus, in agreement with the observations of Ferreira Filho et al. (1998) and with the larger heat production of LS, we have assumed a lower melting degree of the crust in US than in LS. The restitic paragenesis are Pl 30, Gr 20, Sil 10, Qtz 20 Bi 20 in US, and Pl 10, Gr 60, Sil 20, Qtz 10 in LS. On this basis we have estimated bulk partition coefficients, reported in Table 3A and 3B, by using the set of partition coefficients of Bea et al. (1994) except for Sr in plagioclase. From the equations of Blundy and Wood (1991) and Bindeman et al. (1998), assuming plagioclase composition = An 20, $^{Pl}D_{Sr}$ results ~6.8.

7.2. Modelling results

7.2.1. Isotopes

The Niquelândia isotope array is compared with modelled trends in Fig. 4a (LS) and 4b (US). The parameters used in the modelling, explained in the preceding section, are reported in Table 3A and 3B. Points in the model line represent ~5 °C temperature decrease. LS is best approximated by assuming high T_{eq} and partition coefficients for high degree crustal melting. As a consequence of sample spreading (see Section 5), the model variation line cuts through the LS array. By changing input model parameters, the mismatch between single points and model line would obviously persist. Sample spreading may be due in part to analytical uncertainty, but is more likely the result of different magma inputs, corresponding to the various units, and by their mixing with the residual melt of the lower unit. Precise modelling of this item is impossible because the mass of the residual melt, and its consequent degree of contamination, may have any value between the most contaminated sample of the lower unit and residual melt close to complete solidification. The most obvious qualitative consequence is that such a process would result in isotopic values enriched with respect to those of the initial magma, which is consistent with the subparallel arrays of the various units, and at a lower temperature with respect to that of the initial magma, which in modelling would slightly decrease the extent of relative contamination.

The simplified model illustrated in Fig. 4a, anyway, does suggest that it is possible to explain the isotope variations through LS using the xenoliths as the contaminant, whereas the spreading suggest that LS consists of several magma inputs, where the new magma may have mixed with

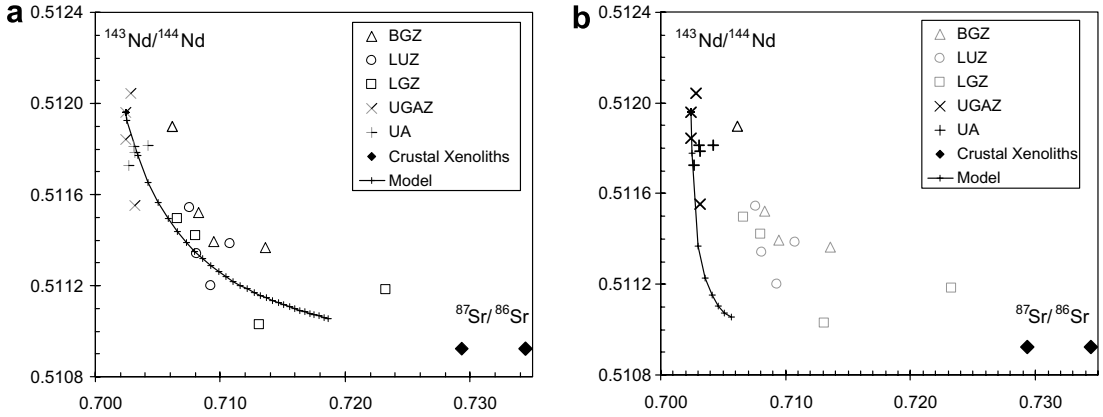

Fig. 4. EC-AFC modelling of the LS (3A) and the US (3B) Sr and Nd isotopic variations. Model parameters are explained in the text and shown in Table 3A and 3B. Ticks on the model lines represent ~5 °C temperature decrease.

the residual melt of the preceding input. In the model presented, assimilation begins when the magma has been cooled to 1098 °C and the crust has been heated up to 851 °C. At this point the cumulate mass (Mc) was 0.5 and the mass of assimilated material with respect to that of cumulates (Ma/Mc) = 0.009. At the end of the process, magma was cooled down to 946 °C and crust heated up to 931 °C, the mass of cumulates was 0.8 and Ma/Mc = 0.43. Higher intrusion temperature of the magma would extend crustal melting and assimilation: rising the temperature from 1250 to 1300 °C would make the isotopic values vary from $^{87}Sr/^{86}Sr = 0.7186$, $^{143}Nd/^{144}Nd = 0.511056$ to $^{7}Sr/^{86}Sr = 0.7206$, $^{143}Nd/^{144}Nd = 0.511031$.

The US isotopic data (Fig. 4b) plot close to the line modelled using the input data in Table 3B (lower T_{eq} and lower crustal melting) and are consistent with a much lower contamination than LS. The most contaminated UGAZ sample approximates the model when the temperature of the magma is 882 °C, that of the crust 854 °C, Mc = 0.94 and Ma/Mc = 0.04. The negligible point spread in UGAZ is probably a consequence of the fact that this unit represents a single magma input.

7.2.2. Trace element–isotope-relationships

The variation of the REE patterns along with the isotopes, qualitatively illustrated in Section 6, indicates that crustal contamination induced a variation of the La_n/Sm_n ratio. The variation of $^{143}Nd/^{144}Nd_{830\ Ma}$ with respect to the whole-rock La_n/Sm_n ratio is compared in Fig. 5a and b with the variations resulting from the model liquids for LS and US. All the LS samples plot in a dispersed array on the left of the model liquid variation line (Fig. 5a). The deviations from the model lines may be explained by the vectors controlling isotopes and trace elements. The isotopic variation of the liquid depends on the respective composition of the initial magma and wall rock and by the contamination process above modelled. The variation of the trace elements is controlled by: (a) the metasomatic process, which would induce an increase of the La_n/Sm_n ratio at increasing contamination; (b) the respective amounts of cumulus crystals and trapped melt in the sample, which would result in variations of the La_n/Sm_n ratio at a given isotopic ratio value. This problem persists even by selecting samples containing the largest number of phases and which might, therefore, approach the equilibrium crystallization of the melt. To illustrate this point, the La_n/Sm_n variation trend with respect to $^{143}Nd/^{144}Nd$ of a Pl50 Cpx50 crystal mixture in equilibrium with the model melts is reported in Fig. 5a. Partition coefficients are reported in the Fig. 5 caption. As expected, the crystal mixture has constantly lower La_n/Sm_n value than that of the coexisting melt. This persists in spite of the large amount of plagioclase (which has higher La_n/Sm_n than the parent melt) in the crystal mixture, as a consequence of the much lower Sm concentration of plagioclase with respect to clinopyroxene. All the LS samples plot around the crystal mixture line and between this and the melt variation lines. They may, therefore, be explained by variable mixtures of cumulate crystals and melt. Because of their low partition coefficients, the addition of olivine and orthopyroxene to the cumulus would have little effect, although it would contribute to a low La_n/Sm_n. The larger distance from the model liquid line of the BGZ and LUZ samples with respect to LGZ suggests that the gabbros of the lower units contain a larger proportion of cumulus crystals, which is also consistent with their generally lower concentration of REE with respect to LGZ (Fig. 3).

The US gabbros and amphibolites plot very close to, or on, the liquid variation line, except anorthosite Niq 1552 which is displaced to the right. This suggests that most samples represent the crystallization result of a polisaturated melt, whereas Niq1552 is consistent with cumulus plagioclase.

The evidence for cumulus plagioclase is better illustrated by using a Pl-compatible element, like Sr. This is done in Fig. 5c and d (LS and US, respectively), where rocks are compared with liquid model lines and model variation of the plagioclase composition by using diagrams $^{87}Sr/^{86}Sr_{830\ Ma}$ vs Sr. The model variation line of the cumulus crystals shows a segment at constant isotope value and

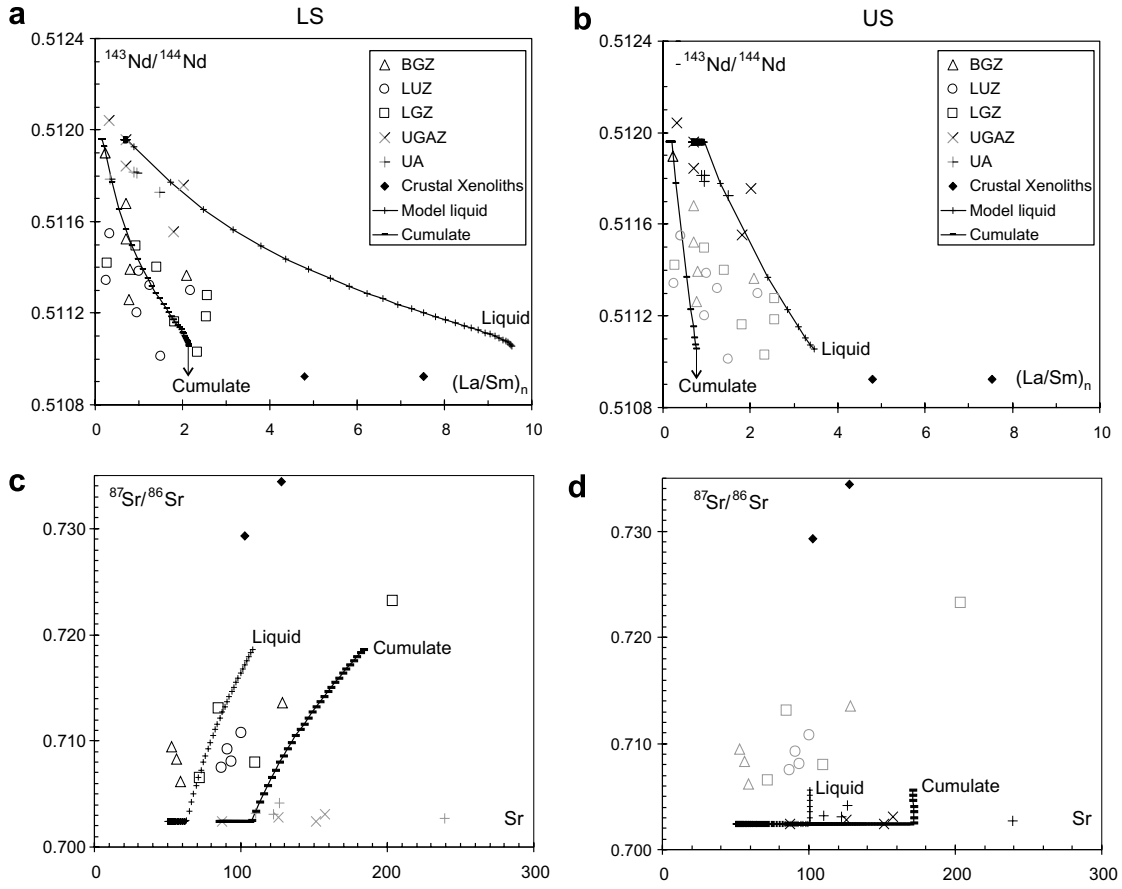

Fig. 5. (a) Variation of $^{143}Nd/^{144}Nd_{830\ Ma}$ with respect to La_n/Sm_n of the LS samples compared with the EC-AFC model variation line of liquids and their equilibrium solid (labelled "cumulate" in the diagram) constituted by Pl50 Cpx50. (b) Similar to (a), but for US. (c) Variation of $^{87}Sr/^{86}Sr_{830\ Ma}$ with respect to Sr (ppm) of the LS samples compared with the EC-AFC model variation line of liquids and their equilibrium plagioclase (labelled "cumulate in the diagram); (d) similar to (c), but for US. In all the diagrams the entire set of Niquelândia samples is reported, but those not directly concerned by the diagram are in grey. partition coefficients used in modelling cumulates: $^{pl}D_{La} = 0.14$, $^{pl}D_{Sm} = 0.08$; $^{cpx}D_{La} = 0.08$; $^{cpx}D_{Sm} = 0.9$ (Henderson, 1984); $^{pl}D_{Sr} = 1.7$ (average partition coefficient of LS and US). Ticks on the model lines represent ~5 °C temperature decrease.

variable Sr concentration: this corresponds to the fractional crystallization of the magma while heating the crust to melting. It shows that very little cumulus plagioclase is sufficient to shift the natural data on the right of the model liquid variation line.

An approach such as that above illustrated is potentially a powerful tool for estimating the amount of cumulus crystals and trapped melts in natural sample. The reliability of such an estimate is, however, dependent on how sharply the input model parameters (mainly the compositions of the magma and of the contaminant) can be constrained.

8. Conclusions

The Sr and Nd isotope variations in the Niquelândia complex provide clear evidence of crustal contamination. The isotopic variation array in LS suggests that each stratigraphic unit corresponds to the inflow of new magma, which mixes with the residual, contaminated melt of the lower unit. This does not exclude that each stratigraphic unit is itself the result of several magma inputs, but the present data are not sufficient to demonstrate this point.

The large melt volume represented in LS induced extensive crustal melting, shown by the highly restitic mineral assemblages in crustal xenoliths, whereas the comparatively smaller US induced lower crustal melting.

Effects of the interaction between the mantle-derived melts and the crustal anatectic melts was a variation of the Sr and Nd isotopes along different trends in LS and US and an enrichment in the hybrid rocks of elements enriched in the crustal component. This is documented by a variation of the REE patterns from LREE-depleted in samples little affected by crustal interference, to-LREE enriched in samples having concomitantly high $^{87}Sr/^{86}Sr$ and low $^{143}Nd/^{144}Nd$.

The interaction between magmas and crustal melts was modelled in terms of an EC-AFC process, taking into account the different heat budget of the larger LS with respect to US. For the model of the two sequences, the same parent magma and the same initial composition of the crust was used, but different compositions of the ana-

tectic melt because the higher heath budget of LS induced higher crustal melting than in US. At the assumed age of 830 Ma, the AC-AFC approach successfully models the observed arrays.

Comparison of the correlations between isotope and La_n/Sm_n and Sr variations in gabbros and EC-AFC model melts permits a qualitative estimation of the relative amount of cumulus crystals and interstitial melts in the gabbros.

The present study shows that both LS and US can be explained as a result of the interaction of the same initial magma with the same crustal component, provided that different environmental conditions are assumed. Future work may provide further data on possible contaminants and permit better constraints on the LS–US relationships and the processes within each unit.

Acknowledgements

This study benefitted from the financial support of the Brazilian Agencies FAPESP (project 04/03022-6) and CNPq and of the Italian MURST (project COFIN 2005). Thanks are due to P. Mori (GMG-IGc-USP XRF Laboratory) for XRF determinations and to M. Sugano Navarro (GMG-IGc-USP Chemistry and ICP Laboratory) for ICP-MS analyses. We thank H.H.G.F. Ulbrich for reviewing the manuscript. The revision of three anonymous reviewers is acknowledged.

References

Asimow, P.D., Ghiorso, M.S., 1998. Algorithmic modifications extending MELTS to calculate Subsolidus Phase Relations. Am. Mineral. 83, 1127–1131.

Bea, F., Pereira, M.D., Stroh, A., 1994. Mineral/leucosome trace-element partitioning in a peraluminous migmatite (a laser ablation-ICP-MS study). In: Foley, A.F., Van Der Laan, S.R. (Eds.) Trace Element Partitioning with Application to magmatic Processes. Chem. Geol. Spec Issue, vol. 117, pp. 291-312.

Bindeman, I.N., Davis, A.M., Drake, M.J., 1998. Ion Microprobe study of plagioclase-basalt partition experiments at natural concentration levels of trace elements. Geochim. Cosmochim. Acta 62, 1175–1193.

Blundy, J.D., Wood, B.J., 1991. Crystal chemical controls on the partitioning of Sr and Ba between plagioclase feldspar, silicate melts, and hydrothermal solutions. Geochim. Cosmochim. Acta 55, 193–209.

Bohrson, W.A., Spera, F.J., 2001. Energy-constrained open-system magmatic processes II: application of Energy-constrained assimilation and fractional crystallization (EC-AFC) model to Magmatic systems. J. Petrology 42, 1019–1041.

Brod, A.J., Jost, H., 1991. Características estruturais, litológicas e magmáticas da zona de cizalhamento dúctil do Rio Trairas, Bloco do Complexo de Niquelândia, Goiás. Rev. Bras. Geoc. 21 (3), 205–207.

Buchanan, D.L., Rouse, J.E., 1984. Role of contamination in the precipitation of sulphides in the Platreef of the Bushveld complex. In: Buchanan, D.L., Jones, M.J. (Eds.), Sulphide Deposits in Mafic and Ultramafic Rocks. Inst. Mining Metallurgy, London, pp. 141–146.

Correia, C.T., Girardi, V.A.V., Lambert, D.D., Kinny, P.D., Reeves, S.J., 1996. 2 Ga U–Pb (SHRIMP II) and Re–Os ages for the Niquelândia basic-ultrabasic layered intrusion, Central Goiás, Brazil. Cong. Bras. Geol., 39, Salvador, Anais SBG 6, 187-189.

Correia, C.T., Jost, H., Tassinari, C.C.G., Girardi, V.A.V., Kinny, P.D., 1999. Ectasian Mesoproterozoic U–Pb ages (SHRIMP II) for the metavolcano—sedimentary sequences of Juscelândia and Indaianópolis and for the high grade metamorphosed rocks of the Barro Alto stratiform igneous complex, Goiás State, Central Brazil. II South American Symp. on Isotopic Geology, Cordoba, Argentina, Actas, pp. 31-33.

Correia, C.T., Girardi, V.A.V., Basei, M A.S., Nutman, A., 2006. Cryogenian U–Pb (Shrimp I) zircon ages of anorthosites from the upper sequences of Niquelândia and Barro Alto Complexes, Central Brazil. *Rev. Bras. Geoc. 36* (Supl. 2) (in press).

DePaolo, D.J., 1981. Trace elements and isotopic effects of combined wallrock assimilation and fractional cristallisation. Earth Planet. Sci. Lett. 53, 189–202.

Eales, H.V., Cawthorn, R.G., 1996. The Bushveld Complex. In: Cawthorn, R.G. (Ed.), Layered Intrusions, Developments in Petrology, vol. 15. Elsevier, Amsterdam-Lausanne-New York-Oxford-Shannon-Tokio, pp. 181–230.

Emeleus, C.H., Cheadle, M.J., Hunter, R.K., Upton, B.G.J., Wadsworth, W.J., 1996. The Rum Layered suite. In: Cawthorn, R.G. (Ed.), Layered Intrusions, Developments in Petrology, vol. 15. Elsevier, Amsterdam-Lausanne-New York-Oxford-Shannon- Tokio, pp. 403–440.

Ferreira Filho, C.F., Kamo, S.L., Fuck, R.A., Krogh, T.E., Naldrett, A.J., 1994. Zircon and rutile U–Pb geochronology in the Niquelândia layered mafic-ultramafic intrusion, Brazil: constraints for the timing of magmatism and high-grade metamorphism. Precambrian Research 68, 241–256.

Ferreira Filho, C.F., Moraes, R., Falcett, J.J., Naldrett, A.J., 1998a. Amphibolite to granulite progressive metamorphism in the Niquelândia Complex, Central Brazil: regional tectonic implications. J. South Amer. Earth Sci. 11, 35–50.

Ferreira Filho, C.F., Naldrett, A.J., Gorton, M.P., 1998b. REE and pyroxene compositional variation across the Niquelândia layered intrusion, Brazil: petrological and metallogenetic implications. Trans. Inst. Min. Metall., Sect. B 107, 1–21.

Ferreira Filho, C.F., Pimentel, M.M., 2000. Sm-Nd isotope systematics and REE data for leucotroctolites and their amphibolitized equivalents of the Niquelândia Complex upper layered series, Central Brazil: further constraints for the timing of magmatism and high-grade metamorphism. J. South Amer. Earth Sci. 13, 647–659.

Fornoni Candia, M.A., Mazzucchelli, M., Siena, F., 1989. Sub-solidus reactions and corona structures in the Niquelândia layered complex (Central Goiás, Brazil). Mineral. Petrol. 40, 17–37.

Fuck, R.A., Brito Neves, B.B., Cordani, U.G., Kawashita, K., 1989. Geocronologia Rb-Sr no complexo Barro Alto, Goiás: evidência de metamorfismo de alto grau e colisão continental há 1300 Ma no Brasil Central. Geochim. Brasiliensis 3, 125–140.

Ghiorso, MS., Sack, R.O., 1995. Chemical mass transfer in magmatic processes. IV.A revised and internally consistent thermodynamic model for the interpolation and extrapolation of liquid-solid equilibria in magmatic systems at elevated temperatures and pressures. Contrib. Mineral. Petrol. 119, 197–212.

Girardi, V.A.V., Rivalenti, G., Sinigoi, S., 1986. The petrogenesis of the Niquelândia layered basic-ultrabasic complex, Central Goiás, Brazil. J. Petrology 27, 715–744.

Girardi, V.A.V., Ferrario, A., Correia, C.T., Diella, V., 2006. A comparison of selected Precambrian Brazilian chromitites: Chromite, PGE-PGM, Re/Os as parental source indicators. J. South Amer. Earth Sci. 20, 303–313.

Girardi, V.A.V., Rivalenti, G., Correia, C.T., Tassinari, C.C.G., Munhá, J.M., Mazzucchelli, M., 2006a. Crustal contamination in the Niquelândia Complex, Central Goias, Brazil: Sr-Nd isotopes and trace-element geochemistry. V South American Symposium on Isotopic Geology, Punta del Este, Uruguay, Short Papers 375-381.

Greeen, T.H., 1994. Experimental studies of trace element partitioning applicable to igneous petrogenesis – Sedona 16 years later. Chemical Geology 117, 1–36.

Henderson, P., 1984. Rare Earth Element GeochemistryDevelopments in Geochemistry, vol. 2. Elsevier, Amsterdam, Oxford, New York, Tokio, pp. 510.

Hofmann, A.W., 1988. Chemical differentiation in the Earth: the relationship between mantle, continental crust and oceanic crust. Earth Planet. Sci. Letters 90, 297–314.

Lee, C.A., 1996. A review on mineralization in the Bushveld Complex and some other Layered Mafic Intrusions. In: Cawthorn, R.G. (Ed.), Layered Intrusions, Developments in Petrology, vol. 15. Elsevier, Amsterdam-Lausanne-New York-Oxford-Shannon- Tokio, pp. 103–146.

McBirney, A.R., 1996. The Skaergaard Intrusion. In: Cawthorn, R.G. (Ed.), Layered Intrusions, Developments in Petrology, vol. 15. Elsevier, Amsterdam-Lausanne-New York-Oxford-Shannon- Tokio, pp. 147–180.

McCallum, I.S., 1996. The Stillwater Complex. In: Layered IntrusionsDevelopments in Petrology, vol. 15. Elsevier, Amsterdam-Lausanne-New York-Oxford-Shannon- Tokio, pp. 441–484.

Moraes, R., Fuck, R.A., Pimentel, M.M., Gioia, S.M.C.L., Figueiredo, A.M.G.F., 2003. Geochemistry and Sm-Nd isotopic characteristics of bimodal volcanic rocks of Juscelândia, Goiás, Brazil: Mesoproterozoic transition from continental rift to ocean basin. Precambrian Research 125, 317–336.

Moraes, R., Fuck, A.R., Pimentel, M.M., Gioia, S.M.C.L., Hollanda, M.H.B.M., Armstrong, R., 2006. The bimodal rift-related volcano-sedimentary sequence in Central Brazil: Mesoproterozoic extension and Neoproterozoic metamorphism. J. South Amer. Earth Sci. 20, 287–301.

Mori, P.E., Reeves, S., Correia, C.T., Haukka, M., 1999. Development of a fused glass disc XRF facility and comparison with the pressed powder pellet technique at Instituto de Geociências, University of São Paulo. Rev. Bras. Geoc. 29, 441–446.

Nascimento, F.S., Veloso, F.D.L.M., Saboia, L.M., 1981. Caracterização e discussão sobre a sequência vulcano-sedimentar da borda oeste do Maciço de Niquelândia (oeste do Rio Trairas). Simp. Geol. Centro-Oeste. Atas SBG, Goiânia, 470–492.

Navarro, M.S., 2004. A implantação de rotina, e seu refinamento, para a determinação de elementos terras raras em materiais geológicos por ICP-OES e ICP-MS. Aplicação ao caso dos granitóides de Pedade-Ibiùna (SP) e Cunhaporanga (PR). M.Sc. thesis, Instituto de Geociencias, Univ. Sao Paulo, 132pp.

Nielsen, F.M., Campbell, I.H., McCullogh, M., Wilson, J.R., 1996. A Strontium isotopic investigation of the Bjerkreim-Sokndal layered intrusion, southwest Norway. J. Petrology 37, 171–194.

Patiño Douce, A.E., Jonhston, A.D., 1991. Phase equilibria and melt productivity in the pelitic system: implications for the origin of peraluminous granitoids and aluminous granulites. Contrib. Mineral. Petrol. 107, 202–218.

Pimentel, M.M., Ferreira Filho, C.F., Amstrong, R.A., 2004. Shrimp U–Pb and Sm-Nd ages of the Niquelândia Layered Complex: Meso- (1.25 Ga) and Neoproterozoic (0.79 Ga) extensional events in Central Brazil. Precambrian Research 132, 132–135.

Pimentel, M.M., Ferreira Filho, C.F., Armele, A., 2006. Neoproterozoic age of the Niquelândia complex, Central Brazil: Further ID-TIMS and Sm-Nd isotopic evidence. J. South Amer. Earth Sci. 21, 228–238.

Rivalenti, G., Girardi, V.A.V., Sinigoi, S., Rossi, A., Siena, S., 1982. The Niquelândia mafic-ultramafic Complex of Central Brazil: petrological considerations. Rev. Bras. Geoc. 12, 380–391.

Sato, K., Tassinari, C.C.G., Kawashita, K., Petronilho, L., 1995. O método geocronológico Sm-Nd no IG/USP e suas aplicações. Annals, Brazilian Academy of Sciences 67, 313–336.

Sinigoi, S., Antonini, P., Demarchi, G., Longinelli, A., Mazzucchelli, M., Negrini, L., Rivalenti, G., 1991. Interactions of mantle and crustal magmas in the southern part of the Ivrea Zone (Italy). Contrib. Mineral. Petrol. 108, 385–395.

Spera, F.J., Bohrson, W.A., 2001. Energy-constrained open-system magmatic processes I: General model and energy-constrained assimilation and fractional crystallization (EC-AFC) formulation. J. Petrology 42, 999–1018.

Taylor, S.R., McLennan, S.M. (Eds.), 1985. The Continental Crust: its Composition and Evolution. Blackwell Scient. Publ., Oxford, London, Edinbugh, Boston, Palo Alto, Melbourne, p. 312.

Vielzeuf, D., Holloway, J.R., 1988. Experimental determination of the fluid-absent melting relations in the pelitic system. Contrib. Mineral. Petrol. 98, 257–276.

Voshage, H., Hofmann, A.W., Mazzucchelli, M., Rivalenti, G., Sinigoi, S., Raczek, I., Demarchi, G., 1990. Isotopic evidence from the Ivrea Zone for a hybrid lower crust formed by magmatic underplating. Nature 347, 731–736.

Wilson, J.R., Robins, B., Nielsen, F.M., Duchesne, J.C., Vander Auwera, J., 1996. The Bjerrkreim-Sokndal Layered Intrusion, Southwest Norway. In: Cawthorn, R.G. (Ed.), Layered Intrusions, Developments in Petrology, vol. 15. Elsevier, Amsterdam-Lausanne-New York-Oxford-Shannon- Tokio, pp. 231–256.

Wilson, J.R., Sorensen, H.S., 1996. The Fongen Hyllingen Layered Intrusive complex, Norway. In: Cawthorn, R.G. (Ed.), Layered Intrusions, Developments in Petrology, vol. 15. Elsevier, Amsterdam-Lausanne-New York-Oxford-Shannon- Tokio, pp. 303–330.